This article has been accepted for publication in a future issue of this journal, but has not been fully edited. Content may change prior to final publication. Citation information: DOI 10.1109/TVT.2014.2385878, IEEE Transactions on Vehicular Technology

Cell Coverage Optimization for the Multicell Massive MIMO Uplink

Shi Jin, *Member, IEEE*, Jue Wang, *Member, IEEE*, Qiang Sun,
Michail Matthaiou, *Senior Member, IEEE*, and Xiqi Gao, *Fellow, IEEE*

***Abstract*—We investigate the cell coverage optimization problem for the massive multiple-input multiple-output (MIMO) uplink. By deploying tilt-adjustable antenna arrays at the base stations, cell coverage optimization can become a promising technique which is able to strike a compromise between covering cell-edge users and pilot contamination suppression. We formulate a detailed description of this optimization problem by maximizing the cell throughput, which is shown to be mainly determined by the user distribution within several key geometrical regions. Then, the formulated problem is applied to different example scenarios: for a network with hexagonal shaped cells and uniformly distributed users, we derive an analytical lower bound of the ergodic throughput in the objective cell, based on which, it is shown that the optimal choice for the cell coverage should ensure that the coverage of different cells does not overlap; for a more generic network with sectoral shaped cells and non-uniformly distributed users, we propose an analytical approximation of the ergodic throughput. After that, a practical coverage optimization algorithm is proposed, where the optimal solution can be easily obtained through a simple one-dimensional line searching within a confined searching region. Our numerical results show that the proposed coverage optimization method is able to greatly increase the system throughput in macrocells for the massive MIMO uplink transmission, compared with the traditional schemes where the cell coverage is fixed.**

***Index Terms*—Cell coverage, massive MIMO, pilot contamination, uplink.**

I. Introduction

Massive multiple-input multiple-output (MIMO) systems (a.k.a. large-scale MIMO) have drawn considerable attention in the literature recently [1]. With a large amount of antennas deployed at the base station (BS), it is possible to achieve very high spectral, as well as, power efficiency with simple linear transceivers [2], [3], e.g., maximum ratio transmission (MRT) and maximum ratio combining (MRC). These attractive features make massive MIMO a promising technique for the next generation of mobile communication systems [4].

According to the law of large numbers for independent and identically distributed (i.i.d.) Rayleigh fading conditions, the impact of uncorrelated noise and intra-cell interference can be completely averaged out with massive MIMO, while the system performance is mainly limited by pilot contamination caused by pilot reuse in adjacent cells [5]. Considering massive MIMO systems working in the time division duplex (TDD) mode,[1] orthogonal pilots are sent from users during the training phase in the uplink, while the BSs perform channel estimation and use the obtained channel state information (CSI) for both uplink reception and downlink transmission. The number of available orthogonal pilots is limited by the length of the channel coherence time. As the number of cells and number of users per cell increase, pilot reuse is inevitable; thus, the uplink channel estimation in one cell will be contaminated by the uplink channels of users from other cells that are using the same pilot sequence. To overcome this intimately negative effect, several works have been documented. Coordinated channel estimation was proposed in [7], while pilot length reducing techniques were discussed in [8]. On the other hand, the issue of pilot reuse and allocating mechanism design was studied in [7], [9], and precoding was investigated in conjunction with pilot contamination in [5], [10].

Different from the above mentioned approaches, we prefigure that pilot contamination can be, alternatively, suppressed from a macroscopic perspective, e.g., the cell coverage. In general, cell coverage adjustment can be realized in practice via antenna tilting techniques. An early contribution on the topic of antenna tilting can be found in [11], which was later extended to universal mobile telecommunications systems (UMTS) [12], long term evolution (LTE) systems [13], [14] and network MIMO systems [15]. The topic of antenna tilt design has been widely studied in recent years [14]–[20], among which self-optimization of tilt angle was investigated in [16]–[18], angle signal strength prediction for downtilted

Manuscript received December 26, 2013; revised July 1 and October 25, 2014. The editor coordinating the review of this paper and approving it for publication was Y. Gong.

S. Jin and X. Gao are with the National Communications Research Laboratory, Southeast University, Nanjing 210096, P. R. China. Emails: {jinshi, xqgao}@seu.edu.cn.

J. Wang and Q. Sun are with the School of Electronic and Information Engineering, Nantong University, Nantong 226019, China. Emails: {wangjue, sunqiang}@ntu.edu.cn. J. Wang is also with Singapore University of Technology and Design, Singapore 138682.

M. Matthaiou is with the School of Electronics, Electrical Engineering and Computer Science, Queen's University Belfast, Belfast, BT3 9DT, U.K., and with the Department of Signals and Systems, Chalmers University of Technology, SE-412 96, Gothenburg, Sweden. Email: m.matthaiou@qub.ac.uk.

This work was supported by National Natural Science Foundation of China under Grants (61401240, 61222102, 61320106003), the Natural Science Foundation of Jiangsu Province under Grant BK2012021, the National Science and Technology Major Project of China under Grant 2013ZX03001032-004, the Program for Jiangsu Innovation Team, and the International Science and Technology Cooperation Program of China under Grant 2014DFT10300.

The work of M. Matthaiou has been supported in part by the Swedish Governmental Agency for Innovation Systems (VINNOVA) within the VINN Excellence Center Chase.

[1]Note that the tremendous CSI feedback overhead makes the frequency division duplex (FDD) mode challenging in massive MIMO systems; for this reason, most relative works on massive MIMO focus on the TDD mode. It should be highlighted that some novel methods have been proposed to implement massive MIMO transmission in the FDD mode, e.g., see [6] and the references therein. However, a detailed comparison of these different duplex modes is beyond the main scope of this paper.

This article has been accepted for publication in a future issue of this journal, but has not been fully edited. Content may change prior to final publication. Citation information: DOI 10.1109/TVT.2014.2385878, IEEE Transactions on Vehicular Technology

antennas was considered in [19], and throughput optimization was studied for multiple input single output (MISO) interference channels [20]. In the literature, it is usually required that the three-dimensional radiation pattern (in dBi) of an antenna element is known, and according to [21], the radiation pattern can be expressed as

$$P|_{\mathrm{dBi}}\left(\beta_{\mathrm{tilt}},\phi,\theta\right) = -\min\left(\min\left[12\left(\frac{\phi-\alpha_{\mathrm{orn}}}{\phi_{\mathrm{3dB}}}\right)^2,\mathrm{SLL}_{\mathrm{az}}\right] + \min\left[12\left(\frac{\theta-\beta_{\mathrm{tilt}}}{\theta_{\mathrm{3dB}}}\right)^2,\mathrm{SLL}_{\mathrm{el}}\right],\mathrm{SLL}_{\mathrm{tot}}\right) + A_{\max} \quad (1)$$

where β_{tilt} is the adjustable tilt angle of the antenna element, while α_{orn} is the fixed orientation angle in the azimuth domain. Moreover, ϕ and θ are the incident angles in the azimuth and elevation domains, respectively. For the azimuth and elevation antenna patterns, ϕ_{3dB} and θ_{3dB} are the half-power beamwidths, while $\mathrm{SLL}_{\mathrm{az}}$ and $\mathrm{SLL}_{\mathrm{el}}$ are the side lobe levels. At last, $\mathrm{SLL}_{\mathrm{tot}}$ is the total side lobe level, and $A_{\max}$ is the peak antenna gain.

To the best of our knowledge, the topic of antenna tilt design in massive MIMO systems remains open for investigation. Recently, exploiting the elevation angular dimension using active antenna arrays in massive MIMO systems has been proposed in [22], where the performance of a technique termed as "full-dimension MIMO (FD-MIMO)", was evaluated using a 3D channel model, assuming different array topologies. However, the authors therein assumed that the number of antennas is not so large, such that pilot contamination is not the dominating factor and can be ignored in the system design. In our work though, we consider an infinitely high number of antennas, therefore, pilot contamination is a dominating design factor in our case. Intuitively, if the coverage areas[2] of different cells are strictly not overlapping, the same set of orthogonal pilots can be reused among cells while causing the least contamination; yet, squeezing the cell coverage without limit will make the coverage of cell-edge users problematic. Thus, considering the trade-off between interference suppression and the coverage of cell-edge users, an optimal cell coverage is expected to exist, which will maximize the cell throughput.[3] Being aware of this, this paper makes the following contributions:

- We derive a generic lower bound of the ergodic cell throughput in the massive MIMO uplink, where the cell coverage is taken into account as an important parameter. We point out that the system performance will be affected by the average number, as well as, the distance distributions of users which are located in several *key regions*, which are defined by the users' locations (described in detail in Definition 1). In parallel, these key regions, and so are the corresponding parameters, will be determined by the cell coverage.
- Considering hexagonal cell shape and uniformly distributed users, we first derive exact analytical expressions for the average number of users, as well as, the probability density functions (PDF) of the distance distribution, for each of the above mentioned key regions. Using these results, the generic lower bound can be specialized; by maximizing this specialized expression, we prove that the optimal strategy of the cell coverage design in this scenario, is to guarantee that the coverage of different cells does not overlap.
- Considering sectoral cell shape and non-uniformly distributed users, we derive exact analytical expressions for the average number of users, as well as, the average user distance, for each of the above mentioned key regions. Using these results, an analytical approximation of the system throughput is proposed, based on which, we are able to further squeeze the searching region of the optimal coverage. It is shown that the system throughput can be efficiently maximized, through one-dimensional line search using the proposed approximation; most importantly, the average throughput can be greatly improved, compared with the setting where the cell coverage is fixed.

The remainder of this paper is organized as follows: The system model is introduced in Section II, the throughput analysis, as well as, the definition of the key regions, are then provided in Section III. Cell overage optimization for uniform and non-uniform user distributions is performed in Section IV and V, respectively. Our numerical results are shown in Section VI, while Section VII concludes the paper.

II. System Model

We consider a three-cell massive MIMO network uplink,[4] where the cell m ($m = 1, 2, 3$) is covered by a BS located at height $h_{\mathrm{BS},m}$, while the BS is being equipped with tilt-adjustable antenna arrays which consist of N antennas. Therefore, there are totally $3N$ antennas in the hexagonal cell. Further, we assume that there are K single-antenna users simultaneously transmitting using space-division-multiple-access (SDMA) in each cell. During the channel training phase, K orthogonal pilots are assigned to the K users in each cell, while the same set of pilots is being reused among all three cells. The system layout is illustrated in Fig. 1, where we use the shaded parts to denote the coverage area of every cell, which is adjustable according to the antenna tilt. Moreover, the radius of the coverage area of the m-th BS is denoted as $r_{\mathrm{BS},m}$, $m = 1, 2, 3$, while the common radius of all cells

[2]In this paper, we ignore the details described by (1), and focus only on the concept of *cell coverage*. In general, if the antenna is designed to have a wide-enough 3-dB main lobe width as well as deep enough attenuation outside of the main lobe, the cell coverage can be directly related with antenna tilting, by inspecting whether a user is located within the main lobe described by (1). This simplification admits more concise mathematical manipulations, as well as, clear physical insights.

[3]In this paper, we only focus on the throughput maximization of the *macro cell*, while the users, which are located in cell-edge areas and cannot be covered by the macro cell, can be alternatively served by small cells [22] or relays [23]. The deployment of small cells or relays requires new design metrics other than the throughput, such as deployment cost and licensing, which, is beyond the main scope of this paper.

[4]Note that the term cell, which we will be using in this paper, will refer to a 120° sector. This is done to avoid introducing additional notation. Nevertheless, our analysis can be readily extended to system layouts where more cells are deployed. With either hexagonal or sectoral shaped cells that will be considered in the subsequent analysis, the three-cell unit represents a baseline topology of larger cells. Thus, later in Fig. 1, we use the widely-used three-sectoral hexagonal cell as an example only for illustration purposes.

This article has been accepted for publication in a future issue of this journal, but has not been fully edited. Content may change prior to final publication. Citation information: DOI 10.1109/TVT.2014.2385878, IEEE Transactions on Vehicular Technology

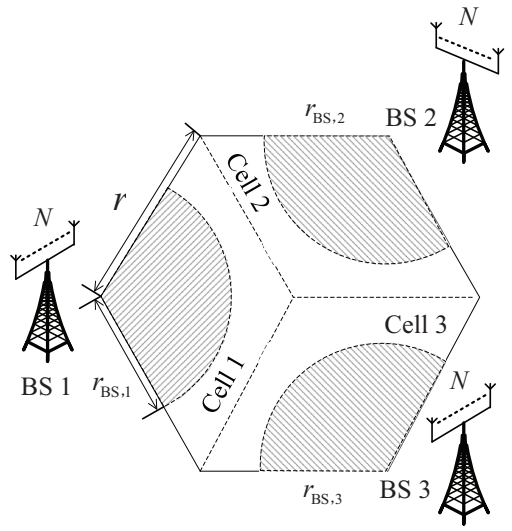

Fig. 1: Layout of a three-cell massive MIMO system.

(which, in this figure, is defined as the distance between the center and the vertex of the hexagon) is denoted as r.

Now, we model the $N \times 1$-sized uplink channel between the BS in cell m, and user k in cell l ($l \in \{1,2,3\}$) as

$$\mathbf{h}_{lk}^{m} = \sqrt{P_{lk}^{m}(\beta_{\mathrm{tilt}}^{m}, \phi_{lk}^{m}, \theta_{lk}^{m})\gamma_{lk}^{m}}\mathbf{g}_{lk}^{m} \tag{2}$$

where $\mathbf{g}_{lk}^{m} \sim \mathcal{CN}(\mathbf{0}_{N\times 1}, \mathbf{I}_{N\times N})$ is the i.i.d. fast fading part of the channel, $\beta_{\mathrm{tilt}}^{m}$ is the tilt angle of BS m, which determines the corresponding coverage, while ϕ_{lk}^{m} and θ_{lk}^{m} are the incident angles of user k in cell l seen by BS m, in the azimuth and elevation domains, respectively. Moreover, $P_{lk}^{m}(\beta_{\mathrm{tilt}}^{m}, \phi_{lk}^{m}, \theta_{lk}^{m})$ is the coefficient of antenna gains, which can be calculated via (1), and γ_{lk}^{m} is the corresponding large-scale fading coefficient caused by path loss, written as

$$\gamma_{lk}^{m} = \frac{C_{\mathrm{PL}}}{(d_{lk}^{m})^{\alpha}} \tag{3}$$

where d_{lk}^{m} is the distance between the k-th user in cell l and the BS in cell m, while α is the path loss coefficient, and C_{PL} is a constant value determined by the path loss model that is used.

According to [2, Eq. (13)], as $N \to \infty$, the asymptotic uplink signal-to-interference ratio (SIR) of user k in cell m can be written as

$$\mathrm{SIR}_{mk}^{\mathrm{uplink}} = \frac{P_{mk}^{m}(\beta_{\mathrm{tilt}}^{m}, \phi_{mk}^{m}, \theta_{mk}^{m})\gamma_{mk}^{m}}{\sum_{l\neq m} P_{lk}^{m}(\beta_{\mathrm{tilt}}^{m}, \phi_{lk}^{m}, \theta_{lk}^{m})\gamma_{lk}^{m}} \tag{4}$$

where the denominator corresponds to the inter-cell interference caused by pilot contamination, assuming the k-th user in cell m and l share the same pilot sequence. Moreover, for the sake of simplicity, we do not consider any power control scheme in (4) and the transmit power from all users is assumed to be the same. The sum-throughput (in bps/Hz) of all three cells is then written as

$$R_{\mathrm{sum}}^{\mathrm{uplink}} = \sum_{m=1}^{3}\sum_{k=1}^{K} \log_2\left(1 + \mathrm{SIR}_{mk}^{\mathrm{uplink}}\right). \tag{5}$$

Note that since a pilot allocation strategy is not considered in this paper, a common term regarding the pilot overhead, namely $\frac{T-T_{\mathrm{pilot}}}{T}$, where T is the block length and T_{pilot} is the training length, is omitted in (5) and henceforth for brevity.

Note that the cell coverage optimization should be implemented in a long term basis which implies that the objective function, i.e. the sum-throughput defined in (5), should be averaged over all possible user locations. On the other hand, the coverage of different cells can be optimized separately for uplink transmission, since the BSs act as receivers, thereby causing no interference to each other in this scenario; as such, we can simply focus on the average throughput of only one cell (denoted as cell m hereafter, without loss of generality), and the optimization problem can be described as

$$\begin{aligned} &\max \mathbb{E}\left[\sum_{k=1}^{K} \log_2\left(1 + \mathrm{SIR}_{mk}^{\mathrm{uplink}}\right)\right] \\ &\text{s.t.} \quad r_{\min} \le r_{\mathrm{BS},m} \le r_{\max} \end{aligned} \tag{6}$$

where $r_{\min}$ and $r_{\max}$ are respectively the minimum and maximum coverage of one BS.

Assumption 1: The following assumptions are made to simplify the analysis. Note that the assumptions stated herein apply only to some special scenarios in our subsequent analysis. Unless otherwise specified, in the following sections, results without making these assumptions are still generic and can be applied to practical scenarios.

1) We assume that the BS hight $h_{\mathrm{BS},m}$ is small compared with the cell radius. As such, the distance from the k-th user in cell l to BS m, i.e., d_{lk}^{m}, is calculated using only the coordinates in the horizontal plane, while $h_{\mathrm{BS},m}$ is ignored in the calculation.[5]
2) Similar to [27, Example 2], here we assume, for the sake of simplicity, that the tilt-adjustable antenna array has uniform gain over the span of its main lobe, i.e., for the users satisfying that $d_{lk}^{m} \le r_{\mathrm{BS},m}$, we let
$$P_{lk}^{m}(\beta_{\mathrm{tilt}}^{m}, \phi_{lk}^{m}, \theta_{lk}^{m}) = 1. \tag{7}$$
On the other hand, for the users located outside of the 3-dB main lobe, according to (1), the antenna gain is constant and can be written as
$$P_{lk}^{m}(\beta_{\mathrm{tilt}}^{m}, \phi_{lk}^{m}, \theta_{lk}^{m}) = -\mathrm{SLL}_{\mathrm{tot}} + A_{\max} \triangleq C. \tag{8}$$
3) Since the value of C_{PL} in (3) will not affect the analysis, hereafter we simply set $C_{\mathrm{PL}} = 1$ for the ease of description.

III. Throughput Analysis

In this section, we analyze the ergodic throughput in cell m, i.e., the objective in (6), aiming at representing it in terms of the user location distributions. This will be the basis of our subsequent coverage analysis. To proceed, we first introduce the following definition:

[5]As will be shown later, cell coverage optimization demonstrates high superiority mainly in the scenarios where most users are located in the cell-edge region. As such, considering a typical cell configuration where the height of the BS is approximately 30m, while the cell radius is 500m, the error caused by this simplification will be small enough to be ignored.

This article has been accepted for publication in a future issue of this journal, but has not been fully edited. Content may change prior to final publication. Citation information: DOI 10.1109/TVT.2014.2385878, IEEE Transactions on Vehicular Technology

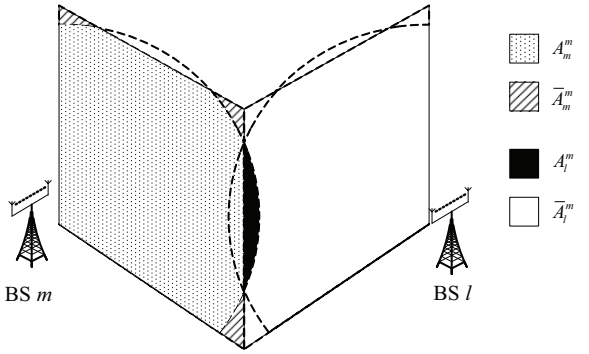

Fig. 2: Illustration of the key regions in Definition 1.

Definition 1: We herein define the following *key regions* (illustrated in Fig. 2):

- A_m^m: The region contains the users in cell m, which are located within the coverage area of the BS in cell m.
- $\bar{A}_m^m$: The region contains the users in cell m, which are located out of the coverage area of the BS in cell m.
- A_l^m: The region contains the users in cell l, which are located within the coverage area of the BS in cell m.
- $\bar{A}_l^m$: The region contains the users in cell l, which are located out of the coverage area of the BS in cell m.

Hereafter, we use $\mathcal{K}_A$ to denote the user set located within region A, while A follows the definitions in Definition 1. The number of users in region A, i.e., the cardinality of $\mathcal{K}_A$, will be denoted as K_A. Note that we have

$$K_{A_m^m} + K_{\bar{A}_m^m} = K \tag{9}$$

$$K_{A_l^m} + K_{\bar{A}_l^m} = K. \tag{10}$$

Moreover, for $k \in \mathcal{K}_{\bar{A}_m^m}$, the corresponding antenna gains P_{mk}^m (we drop the parameters of $P_{mk}^m(\beta_{\text{tilt}}^m, \phi_{lk}^m, \theta_{lk}^m)$ hereafter for brevity) is C, according to item 2) in Assumption 1. Following the same line of reasoning, it also holds that

$$P_{lk}^m \mid_{\text{dBi}} = C, \ k \in \mathcal{K}_{\bar{A}_l^m}. \tag{11}$$

Now, for $k \in \mathcal{K}_{A_m^m}$ or $k \in \mathcal{K}_{\bar{A}_m^m}$, the SIR defined in (4) can be respectively rewritten as

$$\text{SIR}_{mk}^{\text{uplink}} = \frac{N_{m1}}{\sum_{l \neq m}(D_{l1} + D_{l2})}, \ \text{for } k \in \mathcal{K}_{A_m^m} \tag{12}$$

$$\text{SIR}_{mk}^{\text{uplink}} = \frac{N_{m2}}{\sum_{l \neq m}(D_{l1} + D_{l2})}, \ \text{for } k \in \mathcal{K}_{\bar{A}_m^m} \tag{13}$$

where

$$N_{m1} \triangleq P_{mk}^m \gamma_{mk}^m \tag{14}$$

$$N_{m2} \triangleq C\gamma_{mk}^m \tag{15}$$

and

$$D_{l1} \triangleq \Pr\{k \in \mathcal{K}_{\bar{A}_l^m}\} C\gamma_{lk}^m \tag{16}$$

$$D_{l2} \triangleq \Pr\{k \in \mathcal{K}_{A_l^m}\} P_{lk}^m \gamma_{lk}^m. \tag{17}$$

With these definitions, we propose a lower bound for the objective function in (6) in the following theorem:

Theorem 1: For the massive MIMO uplink, the ergodic throughput of cell m can be lower bounded by

$$\begin{aligned} R_{\text{sum},m} &\geq R_{\text{sum},m}^{\text{LB}} \\ &\triangleq K_{A_m^m} \log_2\left(1 + \frac{K}{2\left(K_{\bar{A}_l^m} C\tilde{D}_{l1} + K_{A_l^m}\tilde{D}_{l2}\right)\tilde{N}_{m1}^{-1}}\right) \\ &\quad + K_{\bar{A}_m^m} \log_2\left(1 + \frac{KC}{2\left(K_{\bar{A}_l^m} C\tilde{D}_{l1} + K_{A_l^m}\tilde{D}_{l2}\right)\tilde{N}_{m2}^{-1}}\right) \end{aligned} \tag{18}$$

where

$$\tilde{D}_{l1} \triangleq \mathbb{E}_l\left[\gamma_{lk}^m\right] \mid_{k \in \mathcal{K}_{\bar{A}_l^m}} \tag{19}$$

$$\tilde{D}_{l2} \triangleq \mathbb{E}[P_{lk}^m \gamma_{lk}^m] \mid_{k \in \mathcal{K}_{A_l^m}} \tag{20}$$

$$\tilde{N}_{m1}^{-1} \triangleq \mathbb{E}[(P_{mk}^m \gamma_{mk}^m)^{-1}] \mid_{k \in \mathcal{K}_{A_m^m}} \tag{21}$$

$$\tilde{N}_{m2}^{-1} \triangleq \mathbb{E}[(\gamma_{mk}^m)^{-1}] \mid_{k \in \mathcal{K}_{\bar{A}_m^m}}. \tag{22}$$

Proof: The ergodic throughput in cell m can be rewritten as

$$R_{\text{sum},m} \triangleq \mathbb{E}_{ml}\left[\sum_{k=1}^{K} \log_2\left(1 + \text{SIR}_{mk}^{\text{uplink}}\right)\right] \tag{23}$$

$$\begin{aligned} &= K_{A_m^m}\mathbb{E}_{ml}\left[\log_2\left(1 + \text{SIR}_{k \in A_m^m}\right)\right] \\ &\quad + K_{\bar{A}_m^m}\mathbb{E}_{ml}\left[\log_2\left(1 + \text{SIR}_{k \in \bar{A}_m^m}\right)\right] \end{aligned} \tag{24}$$

where $\mathbb{E}_{ml}[\cdot]$ means taking expectation with respect to the locations of the users within both cells m and l. Note that for $\text{SIR}_{k \in A_m^m}$ and $\text{SIR}_{k \in \bar{A}_m^m}$, their denominators are the same as defined in (12) and (13), while the nominators are different, as defined in (14) and (15), respectively. We also apply (12)–(17) by noting that the probability in (16) and (17) can be calculated as the ratio of number of users within the corresponding region over the total number of users K. Finally, we use the following Jensen's lower bounding technique:

$$\mathbb{E}\left[\log_2\left(1 + \frac{X}{Y}\right)\right] \geq \log_2\left(1 + \frac{1}{\mathbb{E}\left[\frac{Y}{X}\right]}\right). \tag{25}$$

Then, the theorem is directly obtained. ■

Remark 1: Note that Theorem 1 is given in a generic form, where we do not use any of the simplifications declared in Assumption 1. In Theorem 1, the massive MIMO uplink throughput is directly related to long-term statistic parameters, such as the average number of users in every key region, as well as, the distribution of the distance from users to the BS, which are determined by the user location distribution and can be easily obtained at the BS by long-term measuring and estimation. In the following, we will apply Theorem 1 to different typical cell shapes and user distributions, to obtain some analytical results for specific scenarios.

IV. Coverage Optimization for Uniform Distribution of Users

In this section, we specialize the statistical expectation terms in (18) for a typical network structure with hexagonal shaped cells and uniformly distributed users, as described in

This article has been accepted for publication in a future issue of this journal, but has not been fully edited. Content may change prior to final publication. Citation information: DOI 10.1109/TVT.2014.2385878, IEEE Transactions on Vehicular Technology

Assumption 2. After that, the optimal $r_{\mathrm{BS},m}$ is found for this scenario.

Assumption 2 (Uniform Distribution of Users): The shape of the cells and the user locations satisfy

1) The cells are assumed to be hexagonal shaped.
2) All users are assumed to be uniformly distributed in their corresponding cells.

As such, due to the symmetry of this system layout, the optimal coverage areas (i.e., $r_{\mathrm{BS},m}, m = 1, 2, 3$) of all three BSs will be the same. Thus, hereafter in this section, we drop the subscript m in $r_{\mathrm{BS},m}$, and simply use r_{BS} to denote the parameter to be optimized.

A. Parameter Specification for Throughput Analysis

We first specialize the parameters that are needed in calculating (18), in the scenario described by Assumption 2. At first, we evaluate the average number, as well as, the PDF of their distances to BS m, of the users distributed in every key region defined in Definition 1. The results proposed in this subsection will serve as a necessary basis of the subsequent rate analysis.

Proposition 1: With Assumption 2, the average number of users located in every key region defined in Definition 1 can be respectively evaluated as (26) and (27) at the bottom of this page, and

$$K_{\bar{A}_m^m} = K - K_{A_m^m} \tag{28}$$

$$K_{\bar{A}_l^m} = K - K_{A_l^m}. \tag{29}$$

Proof: Under the assumption that the users are uniformly distributed in the cells, the number of users in a region A is proportional to the area of A, thus it can be obtained as

$$K_A = \min\left(K, K\frac{\mathcal{A}(A)}{\mathcal{A}_{\mathrm{cell}}}\right) \tag{30}$$

where $\mathcal{A}(\cdot)$ is the area of a region, while $\mathcal{A}_{\mathrm{cell}}$ is the area of each rhombus cell, which is

$$\mathcal{A}_{\mathrm{cell}} = \frac{\sqrt{3}r_{\mathrm{cell}}^2}{2}. \tag{31}$$

Using (30) and (31), (26) and (27) are obtained using simple but tedious geometrical manipulation methods, while (28) and (29) are obtained by (9) and (10). ■

Proposition 1 provides exact analytical expressions for the average number of uniformly distributed users, for each of the key regions defined in Definition 1. Then, regarding the distributions of d_{lk}^m and d_{mk}^m, the following two lemmas are respectively derived:

Lemma 1: The PDF of the random distance between the vertex of one rhombus and a uniformly distributed node in an adjacent rhombus, sharing the same side but being with different orientation, is written as

$$f_{d_{lk}^m}(x) = \begin{cases} 0, & x < \frac{\sqrt{3}}{2}r \\ \frac{4x}{\sqrt{3}r^2}\arccos\frac{\sqrt{3}r}{2x}, & \frac{\sqrt{3}}{2}r \le x \le r \\ \frac{\pi x}{\sqrt{3}r^2} - \frac{2x}{\sqrt{3}r^2}\arccos\frac{\sqrt{3}r}{2x}, & r < x \le \sqrt{3}r \\ \frac{\pi x}{3\sqrt{3}r^2} - \frac{2x}{\sqrt{3}r^2}\arccos\frac{\sqrt{3}r}{x}, & \sqrt{3}r < x \le 2r \\ 0, & x > 2r. \end{cases} \tag{32}$$

Proof: We use the area-ratio approach used in [25], where the CDF of the distance between one fixed point and a uniformly distributed point in a cell, can be written in the form of the ratio of two corresponding areas. The area of the rhombus cell was determined in (31). On the other hand, the area of A_l^m can be determined separately as in (33) at the bottom of this page. Thus, the CDF of d_{lk}^m can be obtained by noting that $\frac{\mathcal{A}(A_l^m)}{\mathcal{A}_{\mathrm{cell}}}$, as described in (34) (See bottom of the next page), and the corresponding PDF is derived by differentiating (34) with respect to x. ■

Lemma 2: The PDF of the random distance between a uniformly distributed node in a rhombus and its vertex, is

$$K_{A_m^m} = \begin{cases} K\frac{2\pi r_{\mathrm{BS}}^2}{3\sqrt{3}r^2}, & r_{\mathrm{BS}} \le \frac{\sqrt{3}}{2}r \\ 2K\frac{2\left(\frac{\pi}{6} - \arccos\frac{\sqrt{3}r}{2r_{\mathrm{BS}}}\right)r_{\mathrm{BS}}^2 + r\sqrt{3}\sqrt{r_{\mathrm{BS}}^2 - \frac{3}{4}r^2}}{\sqrt{3}r^2}, & \frac{\sqrt{3}}{2}r < r_{\mathrm{BS}} \le r \\ K, & r_{\mathrm{BS}} > r \end{cases} \tag{26}$$

$$K_{A_l^m} = \begin{cases} 0, & r_{\mathrm{BS}} \le \frac{\sqrt{3}}{2}r \\ K\frac{2r_{\mathrm{BS}}^2\arccos\frac{\sqrt{3}r}{2r_{\mathrm{BS}}} - r\sqrt{3}\sqrt{r_{\mathrm{BS}}^2 - \frac{3}{4}r^2}}{\sqrt{3}r^2}, & \frac{\sqrt{3}}{2}r < r_{\mathrm{BS}} \le r \\ K\frac{\left(\sqrt{r_{\mathrm{BS}}^2 - \frac{3}{4}r^2} - \frac{r}{2}\right)\frac{\sqrt{3}}{2}r + \left(\frac{\pi}{2} - \arccos\frac{\sqrt{3}r}{2r_{\mathrm{BS}}}\right)r_{\mathrm{BS}}^2 - \frac{\sqrt{3}}{2}r^2}{\sqrt{3}r^2}, & r < r_{\mathrm{BS}} \le \sqrt{3}r \\ K\frac{\left(\frac{\pi}{6} - \arccos\left(\frac{\sqrt{3}r}{r_{\mathrm{BS}}}\right)\right)r_{\mathrm{BS}}^2 + \sqrt{3}r\sqrt{r_{\mathrm{BS}}^2 - 3r^2}}{\sqrt{3}r^2}, & \sqrt{3}r < r_{\mathrm{BS}} \le 2r \\ K, & r_{\mathrm{BS}} > 2r \end{cases} \tag{27}$$

$$\mathcal{A}\left(A_l^m\right) = \begin{cases} d^2\arccos\frac{\sqrt{3}r}{2d} - \sqrt{d^2 - \frac{3}{4}r^2}\frac{\sqrt{3}r}{2}, & \frac{\sqrt{3}r}{2} \le d \le r \\ \frac{\pi d^2}{4} - \frac{\pi r^2}{6} - \frac{d^2}{2}\arccos\frac{\sqrt{3}r}{2d} + \frac{\sqrt{3}r}{4}\left(\sqrt{d^2 - \frac{3}{4}r^2} - \frac{r}{2}\right), & r < d \le \sqrt{3}r \\ \frac{1}{12}\pi\left(d^2 - 3r^2\right) - \frac{d^2}{2}\arccos\frac{\sqrt{3}r}{d} + \frac{\sqrt{3}r}{2}\sqrt{d^2 - 3r^2}, & \sqrt{3}r < d \le 2r. \end{cases} \tag{33}$$

This article has been accepted for publication in a future issue of this journal, but has not been fully edited. Content may change prior to final publication. Citation information: DOI 10.1109/TVT.2014.2385878, IEEE Transactions on Vehicular Technology

written as

$$f_{d_{mk}^m}(x)=\begin{cases}\frac{4\pi x}{3\sqrt{3}r^2}, & x<\frac{\sqrt{3}r}{2}\\ \frac{4\pi}{3\sqrt{3}r^2}x-\frac{8}{\sqrt{3}r^2}x\arccos\frac{\sqrt{3}r}{2x}, & \frac{\sqrt{3}r}{2}\le x\le r\\ 0, & x>r.\end{cases} \tag{35}$$

Proof: The proof follows the same line of reasoning as that in the proof of Lemma 1. ■

Having the results in Proposition 1, Lemma 1 and Lemma 2 in hand, we are now ready to proceed with deriving analytical expressions for the expectation terms (19)–(22). These results are provided in the following proposition:

Proposition 2: In the typical scenario under Assumption 1 and Assumption 2, the expectation terms (19)–(22) can be analytically evaluated as (36) and (37) at the bottom of this page, where $G_i(x), i=1,2,3$ are respectively defined as

$$G_1(x)\triangleq C_1(\alpha,r)x^{2-\alpha}-2\sum_{n=0}^{\infty}\frac{1}{4^n}C_2(\alpha,n,r)x^{-\alpha-2n+1} \tag{38}$$

$$G_2(x)\triangleq\sum_{n=0}^{\infty}\frac{1}{4^n}C_2(\alpha,n,r)x^{-\alpha-2n+1} \tag{39}$$

$$G_3(x)\triangleq-\frac{C_1(\alpha,r)}{3}x^{2-\alpha}+2\sum_{n=0}^{\infty}C_2(\alpha,n,r)x^{-\alpha-2n+1} \tag{40}$$

where

$$C_1(\alpha,r)\triangleq\frac{1}{2-\alpha}\frac{2\pi}{\sqrt{3}r^2} \tag{41}$$

$$C_2(\alpha,n,r)\triangleq\frac{\binom{2n}{n}3^n r^{2n-1}}{4^n(2n+1)(-\alpha-2n+1)}. \tag{42}$$

On the other hand, $\tilde{N}_{m1}^{-1}$ and $\tilde{N}_{m2}^{-1}$ are respectively written as

$$\tilde{N}_{m1}^{-1}=\frac{\mathcal{A}_{\text{cell}}}{\mathcal{A}\left(A_m^m\right)}\times\begin{cases}H_1(x)\big|_{r_{\min}}^{r_{\text{BS}}}, & r_{\text{BS}}<\frac{\sqrt{3}r}{2}\\ H_1(x)\Big|_{r_{\min}}^{\sqrt{3}r/2}+H_2(x)\Big|_{\sqrt{3}r/2}^{r_{\text{BS}}}, & \frac{\sqrt{3}r}{2}\le r_{\text{BS}}\le r\\ H_1(x)\Big|_{r_{\min}}^{\sqrt{3}r/2}+H_2(x)\Big|_{\sqrt{3}r/2}^{r}, & x>r\end{cases} \tag{43}$$

$$\tilde{N}_{m2}^{-1}=\frac{\mathcal{A}_{\text{cell}}}{\mathcal{A}\left(\bar{A}_m^m\right)}\times\begin{cases}H_1(x)\Big|_{r_{\text{BS}}}^{\sqrt{3}r/2}+H_2(x)\Big|_{\sqrt{3}r/2}^{r}, & r_{\text{BS}}<\frac{\sqrt{3}r}{2}\\ H_2(x)\big|_{r_{\text{BS}}}^{r}, & \frac{\sqrt{3}r}{2}\le r_{\text{BS}}\le r\\ 0, & x>r\end{cases} \tag{44}$$

where $H_1(x)$ and $H_2(x)$ are defined as

$$H_1(x)\triangleq\frac{2}{3}C_1(-\alpha,r)x^{2+\alpha} \tag{45}$$

$$H_2(x)\triangleq\frac{-4}{3}C_1(-\alpha,r)x^{2+\alpha}+\sum_{n=0}^{\infty}\frac{1}{4^{n-1}}C_2(-\alpha,n,r)x^{-2n+\alpha+1}. \tag{46}$$

Proof: See Appendix I. ■

The parameters derived in Proposition 2 are in a complicated form, and so is the corresponding throughput lower bound in Theorem 1; however, the bound expression consists of only elementary functions. Thus, it will be convenient to calculate numerically in practice in a far more efficient manner com-

$$F_{d_{lk}^m}(x)=\begin{cases}0, & x<\frac{\sqrt{3}}{2}r\\ \frac{2x^2}{\sqrt{3}r^2}\arccos\frac{\sqrt{3}r}{2x}-\frac{1}{r}\sqrt{x^2-\frac{3}{4}r^2}, & \frac{\sqrt{3}}{2}r\le x\le r\\ \frac{\pi x^2}{2\sqrt{3}r^2}-\frac{\pi}{3\sqrt{3}}-\frac{x^2}{\sqrt{3}r^2}\arccos\frac{\sqrt{3}r}{2x}+\frac{1}{2r}\left(\sqrt{x^2-\frac{3}{4}r^2}-\frac{r}{2}\right)+\frac{\mathcal{A}(A_l^m)\big|_{r_{\text{BS}}=r}}{\mathcal{A}_{\text{cell}}}, & r<x\le\sqrt{3}r\\ \frac{\pi\left(x^2-3r^2\right)}{6\sqrt{3}r^2}-\frac{x^2}{\sqrt{3}r^2}\arccos\frac{\sqrt{3}r}{x}+\frac{1}{r}\sqrt{x^2-3r^2}+\frac{\mathcal{A}(A_l^m)\big|_{r_{\text{BS}}=\sqrt{3}r}}{\mathcal{A}_{\text{cell}}}, & \sqrt{3}r<x\le 2r\\ 1, & x>2r\end{cases} \tag{34}$$

$$\tilde{D}_{l1}=\frac{\mathcal{A}_{\text{cell}}}{\mathcal{A}\left(\bar{A}_l^m\right)}\times\begin{cases}G_1(x)\Big|_{\sqrt{3}r/2}^{r}+G_2(x)\Big|_{r}^{\sqrt{3}r}+G_3(x)\Big|_{\sqrt{3}r}^{2r}, & r_{\text{BS}}<\frac{\sqrt{3}}{2}r\\ G_1(x)\big|_{r_{\text{BS}}}^{r}+G_2(x)\Big|_{r}^{\sqrt{3}r}+G_3(x)\Big|_{\sqrt{3}r}^{2r}, & \frac{\sqrt{3}}{2}r\le r_{\text{BS}}\le r\\ G_2(x)\Big|_{r_{\text{BS}}}^{\sqrt{3}r}+G_3(x)\Big|_{\sqrt{3}r}^{2r}, & r<r_{\text{BS}}\le\sqrt{3}r\\ G_3(x)\big|_{r_{\text{BS}}}^{2r}, & \sqrt{3}r<r_{\text{BS}}\le 2r\\ 0, & r_{\text{BS}}>2r\end{cases} \tag{36}$$

$$\tilde{D}_{l2}=\frac{\mathcal{A}_{\text{cell}}}{\mathcal{A}\left(A_l^m\right)}\times\begin{cases}0, & r_{\text{BS}}<\frac{\sqrt{3}}{2}r\\ G_1(x)\big|_{\sqrt{3}/2r}^{r_{\text{BS}}}, & \frac{\sqrt{3}}{2}r\le r_{\text{BS}}\le r\\ G_1(x)\Big|_{\sqrt{3}r/2}^{r}+G_2(x)\big|_{r}^{r_{\text{BS}}}, & r<r_{\text{BS}}\le\sqrt{3}r\\ G_1(x)\Big|_{\sqrt{3}r/2}^{r}+G_2(x)\Big|_{r}^{\sqrt{3}r}+G_3(x)\Big|_{\sqrt{3}r}^{r_{\text{BS}}}, & \sqrt{3}r<r_{\text{BS}}\le 2r\\ G_1(x)\Big|_{\sqrt{3}r/2}^{r}+G_2(x)\Big|_{r}^{\sqrt{3}r}+G_3(x)\Big|_{\sqrt{3}r}^{2r}, & r_{\text{BS}}>2r\end{cases} \tag{37}$$

This article has been accepted for publication in a future issue of this journal, but has not been fully edited. Content may change prior to final publication. Citation information: DOI 10.1109/TVT.2014.2385878, IEEE Transactions on Vehicular Technology

pared to time-consuming Monte-Carlo simulations. Numerical results, which we will show later, demonstrate that this lower bound is capable of capturing the exact changing trend of the ergodic sum rate versus $r_{\rm BS}$. As such, it is useful in the subsequent coverage optimization analysis.

B. Coverage Optimization

Based on Theorem 1 and Proposition 2, we obtain the following corollary on the coverage optimization in the considered network with uniform distribution of users:

Corollary 1: With the parameters derived in Proposition 2, the optimal $r_{\rm BS}$ that maximizes the ergodic throughput lower bound proposed in Theorem 1, is written as

$$r_{\rm BS}^{\rm opt} = \frac{\sqrt{3}r}{2}. \tag{47}$$

Proof: See Appendix II. ■

Corollary 1 indicates that for the considered network layout with Assumption 1 and Assumption 2, where the positions of all users are uniformly distributed in hexagonal shaped cells, the benefit gained from enlarging the coverage area of the BS (which means that more edge users will be covered), will be less than the rate loss caused by pilot contamination, which also stems from the coverage area enlargement. Thus, one guideline for cell planning in massive MIMO systems in this scenario, will be that the coverage areas of different cells should not overlap with each other.

Note that the scenario considered in this section, is a simplified ideal model which is not applicable for practical designs. Nevertheless, using this model, we can theoretically showcase the fundamental tradeoff between serving cell-edge users and pilot contamination suppression. For more practical scenarios with non-unit antenna gains and non-uniform user distributions, it can be anticipated that $r_{\rm BS}^{\rm opt}$ may be shifted from $\frac{\sqrt{3}r}{2}$. In the following, we will show for more generic networks, where the users are non-uniformly distributed, that coverage optimization will bring significant throughput gains.

V. Coverage Optimization for Non-Uniform Distribution of Users

It is not surprising that uniform user distribution leads to the conclusion that non-overlapping coverage should be optimal. However, when the users are not uniformly distributed, the optimal coverage should be carefully re-calculated. In this section, we extend the analysis to more general networks with non-uniform user distribution. For the ease of description of this scenario, we also change the cell-shape assumption to be sectoral shaped, which, is also typical and widely adopted in the corresponding literature [26]. The scenario considered in this section is summarized in the following assumption:

Assumption 3 (Non-Uniform Distribution of Users): The cell shape and the user locations distribution are respectively determined as:

1) The cells are assumed to be sectoral shaped.
2) The users are non-uniformly distributed in each cell; also, the user locations's distributions are different among all three cells. This will be described by different number of inner-cell and cell-edge users, as introduced in the following.
3) For the ease of analysis, we further divide a cell into two areas (described in Fig. 3): the inner-cell area (where $d < (\sqrt{3}-1)r$) and the cell-edge area (where $(\sqrt{3}-1)r < d < r$). For cell m, the number of users in these two areas are denoted as $K_m^{\rm inner}$ and $K_m^{\rm edge}$, respectively. As such, we have

$$K = K_m^{\rm inner} + K_m^{\rm edge}. \tag{48}$$

Moreover, we assume that the users are uniformly distributed in these two areas, respectively.

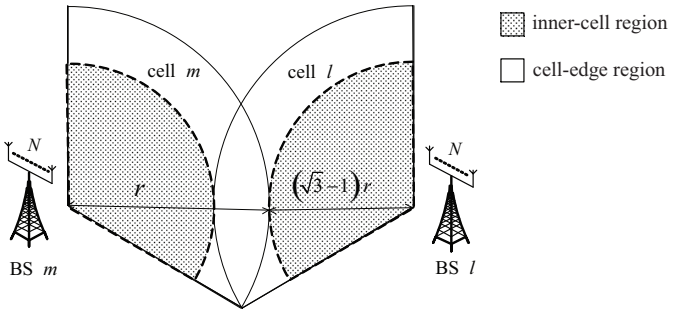

Fig. 3: Illustration of the inner-cell and cell-edge regions.

It is noted that with Assumption 3.3), overlapping occurs only among the cell-edge regions in different cells, while overlapping will not happen for the inner-cell regions. Thus, this definition of cell-edge and inner-cell areas is meaningful and sufficiently realistic in practice.

A. Parameter Specification for Throughput Analysis

Following the same methodology as in Section IV, we first derive exact analytical expressions for the average number of users, as well as, the average distance to BS m, for the users distributed in the key regions defined in Definition 1. These results serve as necessary basis for the following rate analysis.

Proposition 3: With Assumption 3, the average number of users located in every key region defined in Definition 1 can be respectively evaluated as

$$K_{A_m^m} = K_m^{\rm inner} + K_m^{\rm edge}\frac{\alpha_m^2 - (\sqrt{3}-1)^2}{1-(\sqrt{3}-1)^2} \tag{49}$$

$$\begin{aligned} K_{A_l^m} = K_l^{\rm edge}\frac{3}{\pi}\frac{1}{1-\left(\sqrt{3}-1\right)^2}\Bigg(&\alpha_m^2\arccos\frac{\alpha_m^2+2}{2\sqrt{3}\alpha_m} \\ &- \frac{\alpha_m^2+2}{12}\sqrt{12\alpha_m^2-\left(\alpha_m^2+2\right)^2} \\ &+ \arccos\frac{4-\alpha_m^2}{2\sqrt{3}} - \frac{4-\alpha_m^2}{12}\sqrt{12-\left(4-\alpha_m^2\right)^2}\Bigg) \end{aligned} \tag{50, 51}$$

where we define $\alpha_m \triangleq \frac{r_{{\rm BS},m}}{r}$ for brevity. Moreover, we have

$$K_{\bar{A}_m^m} = K - K_{A_m^m} \tag{52}$$

$$K_{\bar{A}_l^m} = K - K_{A_l^m}. \tag{53}$$

Proof: Denoting the area of the inner-cell region as $\mathcal{A}_{\rm inner}$, and the area of the cell-edge region as $\mathcal{A}_{\rm edge}$, we can

This article has been accepted for publication in a future issue of this journal, but has not been fully edited. Content may change prior to final publication. Citation information: DOI 10.1109/TVT.2014.2385878, IEEE Transactions on Vehicular Technology

respectively evaluate them as

$$\mathcal{A}_{\text{inner}} = \frac{\pi\left(\sqrt{3}-1\right)^2}{3} r^2 \tag{54}$$

$$\mathcal{A}_{\text{edge}} = \frac{\pi}{3}\left(1-\left(\sqrt{3}-1\right)^2\right) r^2. \tag{55}$$

On the other hand, using simple geometry, we can get

$$\mathcal{A}(A_m^m) = \frac{\pi\alpha_m^2 r^2}{3} \tag{56}$$

$$\mathcal{A}(A_l^m) \tag{57}$$

$$= r^2\Bigg(\alpha_m^2 \arccos\frac{\alpha_m^2+2}{2\sqrt{3}\alpha_m} - \frac{\alpha_m^2+2}{12}\sqrt{12\alpha_m^2-(\alpha_m^2+2)^2} + \arccos\frac{4-\alpha_m^2}{2\sqrt{3}} - \frac{4-\alpha_m^2}{12}\sqrt{12-(4-\alpha_m^2)^2}\Bigg) \tag{58}$$

Then, the number of users in each region can be respectively calculated as

$$K_{A_m^m} = K_m^{\text{inner}} + K_m^{\text{edge}}\frac{\mathcal{A}\left(A_m^m\right)-\mathcal{A}_{\text{inner}}}{\mathcal{A}_{\text{edge}}} \tag{59}$$

$$K_{A_l^m} = K_l^{\text{edge}}\frac{\mathcal{A}\left(A_l^m\right)}{\mathcal{A}_{\text{edge}}}. \tag{60}$$

Following the same line of reasoning as that used in proving Proposition 1, and using simple geometry, the proposition can be proved. ■

In the following proposition, we derive the average distance from the users distributed in every key region to BS m.

Proposition 4: With Assumption 3, and for the users distributed in every key region defined in Definition 1, their average distance to BS m can be respectively evaluated as

$$d_m^m = \frac{K_{\text{inner}}}{K_{A_m^m}}\frac{2}{3}\left(\sqrt{3}-1\right)r + \left(1-\frac{K_{\text{inner}}}{K_{A_m^m}}\right)\frac{2}{3}\frac{\alpha_m^3-(\sqrt{3}-1)^3}{\alpha_m^2-(\sqrt{3}-1)^2}r \tag{61}$$

$$\bar{d}_m^m = \frac{2}{3}\frac{1-\alpha_m^3}{1-\alpha_m^2}r \tag{62}$$

where $d_m^m \triangleq \mathbb{E}\left[d_{mk}^m\right]$ for all $k \in \mathcal{K}_{A_m^m}$, is the average distance from the users located in region A_m^m to BS m, while $\bar{d}_m^m$, d_l^m and $\bar{d}_l^m$ are similarly defined. For the two terms d_l^m and $\bar{d}_l^m$, their expressions become extremely complicated in this generic scenario, thus are omitted here; nevertheless, we will give a brief description on the corresponding calculation of these two terms, in the proof of this proposition.

Proof: See Appendix III. ■

The results from Proposition 3 and Proposition 4 are now directly applied to the rate analysis. Note that the assumption of non-uniform distribution of users makes the optimization of $r_{\text{BS},m}$ much more complicated than that in the uniformly-distributed scenario. For this reason, instead of using the lower bounding technique in Theorem 1, we hereafter make use of an approximation of $R_{\text{sum},m}$, which is given in the following proposition:

Proposition 5: For the massive MIMO uplink, the ergodic sum rate of the users in cell m can be approximated by (63) at the bottom of this page, where the average number of users $K_{A_m^m}$, $K_{\bar{A}_m^m}$, $K_{A_l^m}$ and $K_{\bar{A}_l^m}$ are defined in Proposition 3, while the average distances d_m^m, $\bar{d}_m^m$, d_l^m and $\bar{d}_l^m$ can be obtained via Proposition 4.

Proof: The proposition is obtained by simply replacing the random distance terms in the SIR term in (24), with their statistical expectations. ■

It is noted that (63) is a generic result, which is not restricted to particular cell shapes.[6] Further applying Proposition 2 and Proposition 3 to (63), the derived result still consists of only elementary functions, thus can be conveniently calculated in practice. Most importantly, our numerical results in Section VI will show that using the rate approximation in Proposition 5 for cell optimization can provide significant throughput gains.

B. Coverage Optimization

The rate approximation proposed in Proposition 5 is still too complicated for the derivation of the exact optimal solution of $r_{\text{BS},m}$. However, as aforementioned, it consists of only elementary functions, thus the optimal $r_{\text{BS},m}$ can be conveniently obtained through one-dimensional line searching. Moreover, with the help of (63), the searching range of the optimal $r_{\text{BS},m}$ can be further squeezed, thereby making the implementation of cell coverage optimization more feasible in practice. As a starting point and, without loss of generality, we can make the following generic assumption that d_{lk}^m is distributed in a range bounded as:[7]

$$d_{l,\min}^m \le d_{lk}^m \le d_{l,\max}^m. \tag{64}$$

Similarly, for d_{mk}^m we assume

$$0 \le d_{mk}^m \le d_{m,\max}^m. \tag{65}$$

[6]The parameters in (63) can be calculated with Assumption 3. However, (63) itself is generic.

[7]The assumption that $\min\limits_{l,l\neq m} d_{l,\min}^m < d_{m,\max}^m$ is reasonable in practice. For example, in the network described in Fig. 2, where hexagon shaped cells are assumed, we have $d_{l,\min}^m = \frac{\sqrt{3}r}{2}$ and $d_{m,\max}^m = r$; while in Fig. 3, where sector shaped cells are considered, we have $d_{l,\min}^m = (\sqrt{3}-1)r$ and $d_{m,\max}^m = r$.

$$R_{\text{sum},m} \approx R_{\text{sum},m}^{\text{approx}} \triangleq K_{A_m^m}\log_2\left(1+\frac{\left(d_m^m\right)^{-\alpha}}{\sum\limits_{l\neq m}\left(K_{A_l^m}\left(d_l^m\right)^{-\alpha}+K_{\bar{A}_l^m}C\left(\bar{d}_l^m\right)^{-\alpha}\right)}\right) + K_{\bar{A}_m^m}\log_2\left(1+\frac{C\left(\bar{d}_m^m\right)^{-\alpha}}{\sum\limits_{l\neq m}\left(K_{A_l^m}\left(d_l^m\right)^{-\alpha}+K_{\bar{A}_l^m}C\left(\bar{d}_l^m\right)^{-\alpha}\right)}\right) \tag{63}$$

This article has been accepted for publication in a future issue of this journal, but has not been fully edited. Content may change prior to final publication. Citation information: DOI 10.1109/TVT.2014.2385878, IEEE Transactions on Vehicular Technology

Algorithm 1 Practical cell coverage optimization

1. Set $K_A = 0, d_A = 0$. Set $t = 0, T_{\rm stat} = T_0$, where T_0 is a predefined time interval for updating the cell coverage;
2. When a user k gets accessed, let $K_A = K_A + 1, d_A = d_A + d_k$ if $k \in \mathcal{K}_A$ (d_k is the distance from user k to the objective BS);
3. When $t = T_{\rm stat}$, calculate the average distance $\bar{d}_A = \frac{d_A}{K_A}$. Then, use Proposition 5 and Corollary 2 to determine the optimal coverage;
4. Compare the values of K_A with that in the prior loop. If the change is significant (e.g., greater than $\alpha_{\rm th}\%$ where $\alpha_{\rm th}$ is a predefined threshold), reduce T_0; similarly, if the change is non-significant, maintain or enlarge the value of T_0 in Step 1 and start the new loop.

Then, the following corollary can be obtained:

Corollary 2: The optimal $r_{{\rm BS},m}$, which maximizes the ergodic uplink sum rate approximation (63), will be within the interval

$$\min_{l,l\neq m} d^m_{l,\min} \leq r^{\tt opt}_{{\rm BS},m} \leq d^m_{m,\max}. \tag{66}$$

Proof: From (63), it is clear that when $r_{{\rm BS},m} > d^m_{m,\max}$, the terms $K_{A^m_m}$, $\bar{K}_{A^m_m}$, as well as, d^m_m and $\bar{d}^m_m$ will be fixed. As such, if $r_{{\rm BS},m}$ keeps enlarging, the only term which will be affected in (63) will be the interference term caused by pilot contamination, i.e., $D \triangleq \sum_{l\neq m}\left(K_{A^m_l}(d^m_l)^{-\alpha} + K_{\bar{A}^m_l} C\left(\bar{d}^m_l\right)^{-\alpha}\right)$ in the denominator. As such, $R_{{\rm sum},m}$ will be decreasing with respect to $r_{{\rm BS},m}$. On the other hand, when $r_{{\rm BS},m} < \min\limits_{l,l\neq m} d^m_{l,\min}$, the interference term D in (63) will be fixed; as such, it is easy to shown that $R_{{\rm sum},m}$ will be increasing with respect to $r_{{\rm BS},m}$ in this regime. ■

As a conclusion of this section, Proposition 5 provides an effective objective function while Corollary 2 further squeezes the searching range within which this objective function can be maximized. With these results in hand, the optimal $r_{{\rm BS},m}$ can be easily found by simple one-dimensional line searching techniques. Based on Proposition 5 and Corollary 2, we propose a cell coverage optimization scheme which can be easily implemented in practice, as described in Algorithm 1. Our numerical results will show that the proposed scheme significantly improves the system throughput, compared with fixed cell coverage.

VI. Numerical Results

As a necessary basis of the subsequent simulations, we first need to numerically validate the results derived in Lemmas 1, 2, as well as, the results in Propositions 1, 3, and 4. At first, the CDFs of d^m_{mk} and d^m_{lk} are shown in Fig. 4, where the cell radius is set to be $r = 500$m, and the curves are respectively obtained by both Monte-Carlo simulations and the analytical expressions in Lemmas 1 and 2. An exact match between the Monte-Carlo and the analytical results can be observed. Recalling the proofs of Lemma 1, Lemma 2 and Proposition 1, the average numbers of users described in (26) and (27), can be directly related to the PDFs described in (32) and (35). As a consequence, Fig. 4 also does prove the accuracy of Proposition 1.

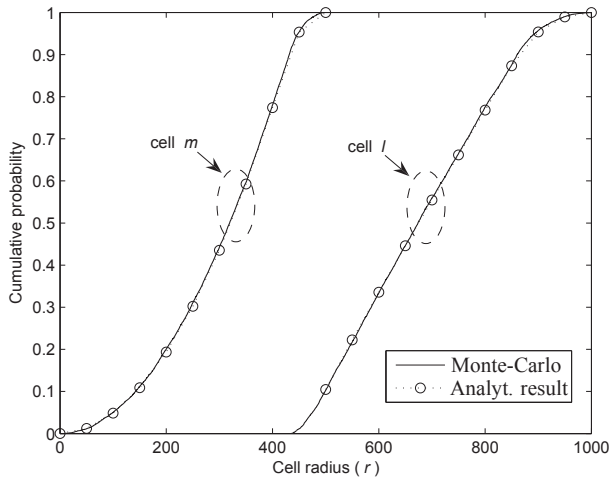

Fig. 4: CDF of d^m_{mk} and d^m_{lk} in a network with hexagonal shaped cells and uniformly distributed users.

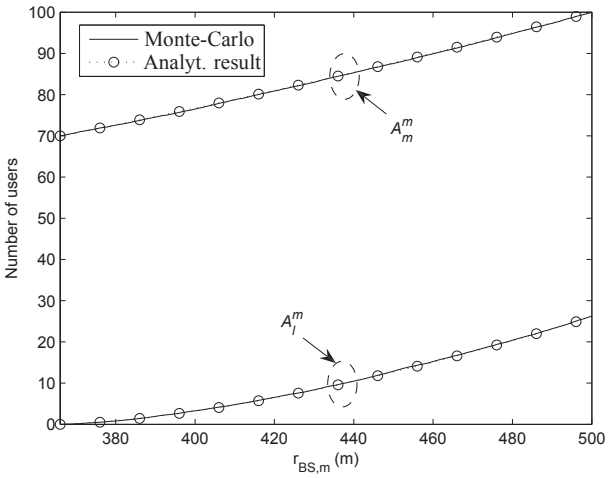

Fig. 5: The average number of users vs. $r_{{\rm BS},m}$ in a network with sectoral shaped cells and non-uniformly distributed users.

Then, we validate Proposition 4 by depicting the average number of users in regions A^m_m and A^m_l, versus the value of $r_{{\rm BS},m}$ in Fig. 5. We set $r = 500$m and $K = 100$ in the simulation. Again, a perfect match between the Monte-Carlo and analytical results is shown. Moreover, as $r_{{\rm BS},m}$ increases, the average numbers of users in regions A^m_m and A^m_l are both increasing, which indicates that while serving more users in cell m, BS m will face more interference from cell l. As a consequence, an optimum coverage which is able to strike a compromise between these contradicting effects does exist, as will be shown later.

In Fig. 6, we compare the Monte-Carlo result with the lower

This article has been accepted for publication in a future issue of this journal, but has not been fully edited. Content may change prior to final publication. Citation information: DOI 10.1109/TVT.2014.2385878, IEEE Transactions on Vehicular Technology

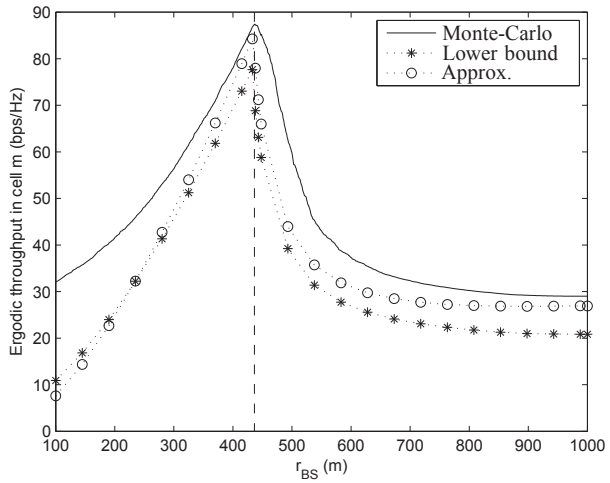

Fig. 6: Ergodic throughput in cell m vs. $r_{\rm BS}$ in a network with hexagonal shaped cells and uniformly distributed users.

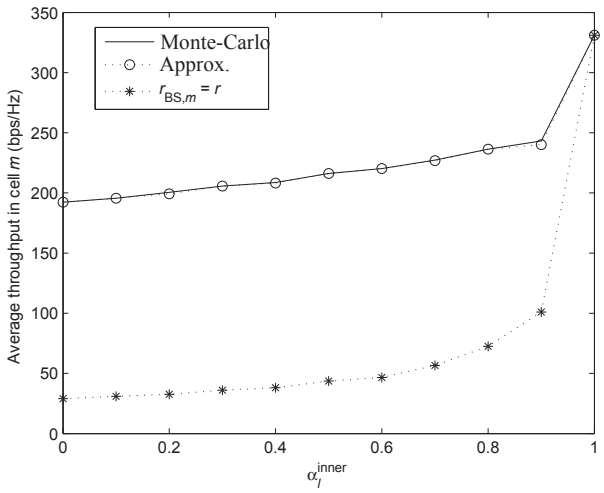

Fig. 7: Throughput in cell m vs. $\alpha_l^{\rm inner}$ in a network with sectoral shaped cells and non-uniformly distributed users.

bound (Theorem 1) and the approximation (Proposition 5) of the ergodic throughput in cell m, vs. the coverage area of the BSs, i.e., $r_{\rm BS}$. In the simulation, we set $r = 500$m, $K = 10$. Assuming unit power gains within the BS coverage area and -20dB outside that coverage, the Monte-Carlo result is calculated directly using the SIR definition in (4), averaged over 500 times of random generations of the users' positions. It is shown that the lower bound, as well as, the approximation are able to reflect the same changing trend as the Monte-Carlo result, thus are qualified to be used in the coverage optimization design. Note that the tightness of the lower bound is different at different values of $r_{\rm BS}$; this is because the bounding technique in (25) has been respectively applied to two weighted terms as shown in (24); with different value of $r_{\rm BS}$, the weight of these two terms, namely $K_{A_m^m}$ and $\bar{K}_{A_m^m}$, will be different, thus leading to different tightness of the combined lower bound. Nevertheless, it is shown that all curves achieve their maximum at the same value of $r_{\rm BS}$, which is about 433m as shown in the figure. This result, which is in fact $\frac{\sqrt{3}}{2}r$, coincides perfectly with our analysis and the results drawn in Corollary 1.

In Fig. 7, the achievable uplink throughput in cell m is depicted versus $\alpha_l^{\rm inner}$, where

$$\alpha_l^{\rm inner} \triangleq \frac{K_l^{\rm inner}}{K} \tag{67}$$

is the parameter indicating the user distribution in cell l. When $\alpha_l^{\rm inner} = 1$, it means that all users in cell l are located in the inner-cell regions, thereby causing the least pilot contamination to the users in cell m; on the other hand, when $\alpha_l^{\rm inner} = 0$, all users in cell l are located in the cell-edge region, and the system performance will be severely degraded by pilot contamination. In the simulation, we assume that the users in cell m are uniformly distributed, i.e., $\alpha_m^{\rm inner} = \frac{\mathcal{A}_{\rm inner}}{\mathcal{A}_{\rm cell}}$. In the figure, different results are shown when the cell coverage is fixed to be $r_{{\rm BS},m} = r$, for $m = 1, 2, 3$, as well as, the setting where the cell coverage is adjustable according to the changing of the user distributions, i.e., $\alpha_l^{\rm inner}$. Moreover, for the coverage-adjustable setting, we compare the Monte-Carlo result (where the searching is carried out directly using (23)) and the one-dimensional line searching using the approximation proposed in Proposition 5. It is shown that (63) in Proposition 5 is a very effective metric, which leads to nearly the same global optimum achieved by tedious Monte-Carlo simulation. Most importantly, the graph demonstrates that coverage optimization results in significant gains in the system throughput, compared with the conventional setting where the coverage is fixed. Specifically, when the value of $\alpha_l^{\rm inner}$ is small, i.e., more interfering users are located in the cell-edge regions of the adjacent cells, the gains brought by cell coverage optimization become substantial. As anticipated, when $\alpha_l^{\rm inner}$ grows large, the benefits of coverage optimization are decreasing, since pilot contamination vanishes.

We now show the optimal cell coverage for different user distribution conditions, determined by both $\alpha_m^{\rm inner}$ and $\alpha_l^{\rm inner}$ in Fig. 8. The results indicate that when the number of cell-edge users increases in adjacent cells, i.e., when $\alpha_l^{\rm inner}$ decreases, the optimal coverage of cell m should be reduced. On the other hand, with increasing $\alpha_m^{\rm inner}$, i.e., more inner-cell users in cell m, the optimal coverage of cell m also decreases. Note that the optimal coverage is always less than $r = 500$m, which confirms our conclusion drawn from Corollary 2. Essentially, it indicates that if the throughput is maximized for the macro cells, the cell-edge users, which are located in the center region of the three-cell unit shown in Fig. 3, will not be covered by any of these cells. As such, small cell stations are necessary to be placed in this area to provide seamless coverage of the entire network.

At last, we apply the cell coverage optimization Algorithm 1 to a practical network, where a typical 19-cell network is considered, as shown in Fig. 9. In the figure, we use black dots to denote the positions of the BSs, each consisting of three 120° sectoral antenna arrays implemented with large but finite number of antennas, i.e., from 100 to 500. In

This article has been accepted for publication in a future issue of this journal, but has not been fully edited. Content may change prior to final publication. Citation information: DOI 10.1109/TVT.2014.2385878, IEEE Transactions on Vehicular Technology

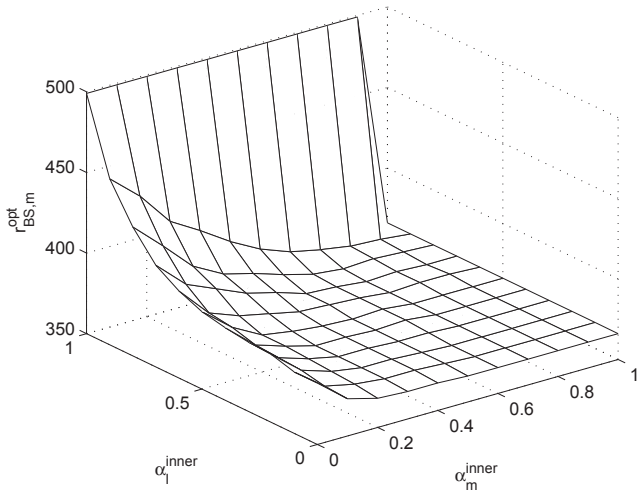

Fig. 8: Optimal cell coverage vs. α_l^{inner} and α_m^{inner} in a network with sectoral shaped cells and non-uniformly distributed users.

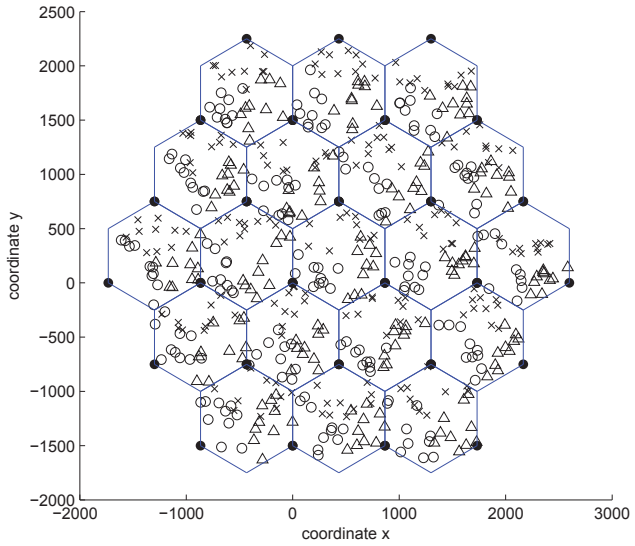

Fig. 9: Layout of the 19-cell network with randomly located users.

every sector, 10 users are non-uniformly located and the users belong to different sectors are described respectively using circle, triangle and x-mark in the figure. The user location distribution is determined by the number of inner-cell and cell-edge users as described in Fig. 3, which, are independently and randomly generated among different sectors as well as different simulation trials.

In Fig. 10, we evaluate the average throughput of the central cell among all 19 cells using Monte-Carlo simulation. The throughput is plotted versus increasing number of antennas. As a benchmark, a reference coverage determination method (labeled as "no overlap" in the figure), which simply determines the coverage of every sector to avoid overlapping, is

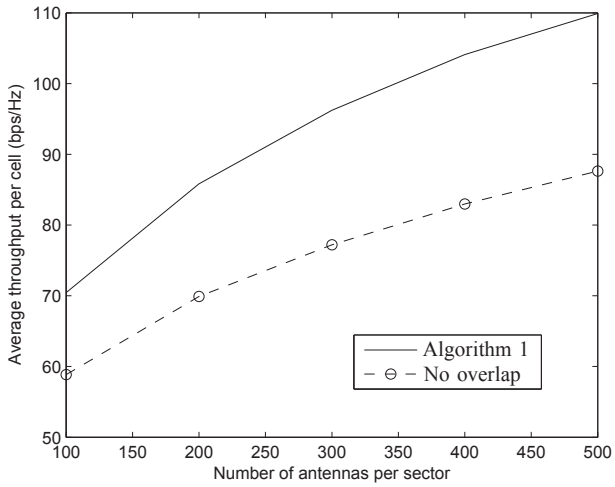

Fig. 10: Average throughput per cell vs. number of antennas per sector.

also illustrated. It is shown that the proposed cell coverage optimization algorithm significantly increases the throughput. As anticipated, the throughput increment gets larger as the number of antenna increases, for the reason that our algorithm is designed based on the asymptotic rate approximation with an infinite number of antennas.

As a last comment, we emphasize the impact of number of antennas on our proposed algorithm. With the assumption of an infinite number of antennas, interference only comes from pilot contamination caused by the users who are using the same pilot in adjacent cells (or sectors). On the other hand, with finite number of antennas, interference also comes from 1) the other users in the same cell, and 2) all users in adjacent cells (assuming a frequency reuse factor 1). Since our algorithm is based on the asymptotic assumption, the finite-antenna interference is ignored in the design. However, we note that with large but finite number of antennas (such as 100–500 as shown in Fig. 10), the mutual interference between two independent wireless links is anyways very small (albeit not zero, which, only holds for the extreme case). In this finite antenna regime, considering only the pilot-contaminating user, other than all users in adjacent cells, is a reasonable choice when performing cell coverage optimization. Although the achievable throughput is much less than that of the infinite-antenna case, the result in Fig. 10 clearly shows that significant gains can still be realized by the proposed algorithm with large but finite number of antennas.

VII. Conclusions

In this paper, cell coverage optimization was investigated in the massive MIMO uplink. We first formulated a detailed description of this important optimization problem, where it was pointed out that the system throughput will be determined by the user distributions in some key geometrical regions. The formulated problem was then applied to different practical scenarios. For a network with hexagonal shaped cells and uniformly distributed users, an analytical lower bound of the

This article has been accepted for publication in a future issue of this journal, but has not been fully edited. Content may change prior to final publication. Citation information: DOI 10.1109/TVT.2014.2385878, IEEE Transactions on Vehicular Technology

ergodic sum rate in the objective cell was derived, based on which it was proved that the optimal choice for the cell coverage should ensure that the coverage of different cells does not overlap. For a more generic network with sectoral shaped cells and non-uniformly distributed users, we proposed an analytical approximation of the ergodic sum rate; after that, the optimal solution can be easily obtained through a simple one-dimensional line searching within a bounded searching region. Our numerical results showcased that the proposed coverage optimization method can substantially increase the system throughput for the massive MIMO uplink transmission, compared with the traditional scheme where the cell coverage is fixed.

Appendix I
Proof of Theorem 1

Starting with evaluating $\tilde{D}_{l1}$, we have

$$\tilde{D}_{l1} = \int_{d_{\bar{A}_l^m,\min}}^{d_{\bar{A}_l^m,\max}} \mathrm{PL}(x) f_{\bar{A}_l^m}(x)\mathrm{d}x = \int_{r_{\mathrm{BS}}}^{2r} \frac{1}{x^\alpha} f_{\bar{A}_l^m}(x)\mathrm{d}x \tag{68}$$

where $d_{\bar{A}_l^m,\min}$ and $d_{\bar{A}_l^m,\max}$ are the minimum and maximum distances between the users in the region $\bar{A}_l^m$ and BS m, respectively; $\mathrm{PL}(x)$ is the function of path loss defined in (3), while

$$f_{\bar{A}_l^m}(x) \triangleq f_{d_{lk}^m}(x)\Big|_{\text{for } k\in\mathcal{K}_{\bar{A}_l^m}} = \Pr\left(d_{lk}^m = x \mid k \in \mathcal{K}_{\bar{A}_l^m}\right) \tag{69}$$

$$= \frac{\Pr\left(d_{lk}^m = x, k \in \mathcal{K}_{\bar{A}_l^m}\right)}{\Pr\left(k \in \mathcal{K}_{\bar{A}_l^m}\right)} = \frac{f_{d_{lk}^m}(x)}{\mathcal{A}\left(\bar{A}_l^m\right)/\mathcal{A}_{\mathrm{cell}}} \tag{70}$$

is the PDF of d_{lk}^m conditioned on that the objective user is located in the regime $\bar{A}_l^m$. To continue evaluating (68), we make use of Lemma 1, and introduce the infinite series expansion of $\arccos(x)$ such that $\arccos(x) = \frac{\pi}{2} - \sum_{n=0}^{\infty} \frac{\binom{2n}{n} x^{2n+1}}{4^n(2n+1)}$, for the ease of analysis. Then, the indefinite integral of $\frac{1}{x^\alpha} f_{\bar{A}_l^m}(x)$ can be derived as

$$\int \frac{1}{x^\alpha} f_{\bar{A}_l^m}(x)\mathrm{d}x = \begin{cases} 0, & x < \dfrac{\sqrt{3}}{2}r \\ G_1(x), & \dfrac{\sqrt{3}}{2}r \le x \le r \\ G_2(x), & r < x \le \sqrt{3}r \\ G_3(x), & \sqrt{3}r < x \le 2r \\ 0, & x > 2r \end{cases} \tag{71}$$

where $G_i(x), i = 1, 2, 3$ were defined in (38)–(40). Then, (36) can be directly obtained by applying (71) to (68). Note that $\tilde{D}_{l2}$ can be obtained on a similar note.

Then, we seek to evaluate $\tilde{N}_{m1}$ and $\tilde{N}_{m2}$. We first evaluate the following indefinite integral as

$$\int x^\alpha f_{d_m^m}(x)\mathrm{d}x = \begin{cases} H_1(x), & x < \dfrac{\sqrt{3}r}{2} \\ H_2(x), & \dfrac{\sqrt{3}r}{2} \le x \le r \\ 0, & x > r \end{cases} \tag{72}$$

where $H_1(x)$ and $H_2(x)$ were defined in (45) and (46). Then, the following proof follows the same line of reasoning as that used before, which leads us to (43) and (44).

Appendix II
Proof of Corollary 1

First, consider the regime where $r_{\mathrm{BS}} \le \frac{\sqrt{3}r}{2}$, then (18) can be simplified as (73) at the bottom of this page, where $\tilde{C}_1 = 2C\left(G_1(x)|_{\sqrt{3}r/2}^{r} + G_2(x)|_{r}^{\sqrt{3}r} + G_3(x)|_{\sqrt{3}r}^{2r}\right)$ is a constant which is independent of r_{BS}. Then, we investigate the monotonicity of (73) by taking the derivative with respect to r_{BS}. By doing so, it can be shown that in the regime $r_{\mathrm{BS}} \le \frac{\sqrt{3}r}{2}$, $R_{\mathrm{sum},m}^{\mathrm{LB}}$ is monotonously increasing. Similarly, in the regime where $r_{\mathrm{BS}} > \frac{\sqrt{3}r}{2}$, $R_{\mathrm{sum},m}^{\mathrm{LB}}$ is decreasing. The derivation is trivial thus is omitted here.

Appendix III
Proof of Proposition 4

In order to evaluate d_m^m, we first define the following user sets: we use $k_1' \in \mathcal{K}_1$ to denote the users located within the inner-cell region, while using $k_2' \in \mathcal{K}_2$ to denote the users located in the region $A_m^m \cap A_{\mathrm{edge}}$. Then, d_m^m can be written that

$$\begin{aligned} d_m^m \triangleq \mathbb{E}\left[d_{mk}^m\right] &= \Pr\{k \in \mathcal{K}_1 | k \in \mathcal{K}_{A_m^m}\}\mathbb{E}\left[d_{mk_1'}^m\right] \\ &\quad + \Pr\{k \in \mathcal{K}_2 | k \in \mathcal{K}_{A_m^m}\}\mathbb{E}\left[d_{mk_2'}^m\right]. \end{aligned} \tag{74}$$

For user k who is located in region A_m^m, it is easy to show that

$$\Pr\{k \in \mathcal{K}_1 | k \in \mathcal{K}_{A_m^m}\} = \frac{K_{\mathrm{inner}}}{K_{A_m^m}} \tag{75}$$

$$\Pr\{k \in \mathcal{K}_2 | k \in \mathcal{K}_{A_m^m}\} = 1 - \frac{K_{\mathrm{inner}}}{K_{A_m^m}}. \tag{76}$$

On the other hand, the PDF of $d_{mk_1'}^m$ and $d_{mk_2'}^m$ can be obtained using the method introduced in the proof of Lemmas 1 and 2. Then, $\mathbb{E}\left[d_{mk_1'}^m\right]$ and $\mathbb{E}\left[d_{mk_2'}^m\right]$ can be respectively evaluated as

$$\mathbb{E}\left[d_{mk_1'}^m\right] = \frac{2}{3}\left(\sqrt{3}-1\right)r \tag{77}$$

$$\mathbb{E}\left[d_{mk_2'}^m\right] = \frac{2}{3}\frac{\alpha^3 - (\sqrt{3}-1)^3}{1-(\sqrt{3}-1)^2}r. \tag{78}$$

$$R_{\mathrm{sum},m}^{\mathrm{LB}} = K_{A_m^m}\log_2\left(1 + \frac{1}{\tilde{C}_1\frac{\mathcal{A}_{\mathrm{cell}}}{\mathcal{A}(A_m^m)}H_1(x)\,|_{r_{\min}}^{r_{\mathrm{BS}}}}\right) + K_{\bar{A}_m^m} \times \log_2\left(1 + \frac{C}{\tilde{C}_1\frac{\mathcal{A}_{\mathrm{cell}}}{\mathcal{A}(\bar{A}_m^m)}\left(H_1(x)\,|_{r_{\min}}^{\sqrt{3}r/2} + H_1(x)\,|_{\sqrt{3}r/2}^{r}\right)}\right) \tag{73}$$

This article has been accepted for publication in a future issue of this journal, but has not been fully edited. Content may change prior to final publication. Citation information: DOI 10.1109/TVT.2014.2385878, IEEE Transactions on Vehicular Technology

According to (74), (77) and (78), (61) can be obtained. On a similar note, we obtain (62).

The aforementioned derivation of d_m^m and $\bar{d}_m^m$ requires only simple geometrical calculation in sectoral areas. However, for the two regions defined in cell l, i.e., A_l^m and $\bar{A}_l^m$, the corresponding calculation becomes more complicated. In the following, we give a brief introduction to the derivation, while the detailed results will be omitted here, for the reason that they are in very tedious forms while little insight can be provided. At first, with the network layout described by Fig. 3, the area of the region A_l^m defined in Definition 1, can be derived as

$$\mathcal{A}\left(A_l^m\right) = r_{\mathrm{BS},m}^2 \cdot \theta - \frac{r_{\mathrm{BS},m}^2 + 2r^2}{2\sqrt{3}r} \cdot h + r^2 \cdot \phi - \left(\sqrt{3}r - \frac{r_{\mathrm{BS},m}^2 + 2r^2}{2\sqrt{3}r}\right) \cdot h \quad (79)$$

where

$$\theta \triangleq \arccos\left(\frac{r_{\mathrm{BS},m}^2 + 2r^2}{2r_{\mathrm{BS},m}\sqrt{3}r}\right) \quad (80)$$

$$\phi \triangleq \arccos\left(\frac{4r^2 - r_{\mathrm{BS},m}^2}{2\sqrt{3}r^2}\right) \quad (81)$$

$$h \triangleq r_{\mathrm{BS},m} \sin\theta. \quad (82)$$

On the other hand, the area of the overlapping region described in Fig. 3 can be calculated as

$$\mathcal{A}_{\mathrm{overlap}} \triangleq \left(\frac{\pi}{3} - \frac{\sqrt{3}}{2}\right) r^2. \quad (83)$$

Assuming that $r_{\mathrm{BS},m}$ falls into the cell-edge region, the CDF of d_{lk}^m, which is the random distance from the user distributed in region A_l^m to BS m, can be written as

$$F_{d_{lk}^m}(x) = \frac{\mathcal{A}\left(A_l^m\right)|_{r_{\mathrm{BS},m}=x}}{\mathcal{A}_{\mathrm{overlap}}}. \quad (84)$$

Taking the derivative of (84) with respect to x, we get the PDF of d_{lk}^m. After that, the analytical expression of d_l^m can be calculated as

$$d_l^m = \int_{(\sqrt{3}-1)r}^{r_{\mathrm{BS},m}} x f_{d_{lk}^m}(x) \mathrm{d}x. \quad (85)$$

At last, the term $\bar{d}_l^m$ depends on both the inner-cell and cell-edge regions, which makes a direct calculation even more challenging. As such, we make the following simplification in the derivation: in the considered network layout, it is reasonable to assume that the average distances to BS m from the users within either the inner-cell regions, or the cell-edge regions, are pre-known system parameters, and we denote them as $d_{l,\mathrm{edge}}^m$ and $d_{l,\mathrm{inner}}^m$ respectively in the following. Then, the average distance to BS m, from all users in cell l, can be obtained as

$$d_{l,\mathrm{cell}}^m \triangleq \frac{1}{K}\left(K_l^{\mathrm{edge}} d_{l,\mathrm{edge}}^m + K_l^{\mathrm{inner}} d_{l,\mathrm{inner}}^m\right). \quad (86)$$

On the other hand, $d_{l,\mathrm{cell}}^m$ can be alternatively evaluated as

$$d_{l,\mathrm{cell}}^m = \frac{1}{K}\left(K_{A_l^m} d_l^m + K_{\bar{A}_l^m} \bar{d}_l^m\right). \quad (87)$$

As such, once d_l^m is obtained through (85), we can obtain $\bar{d}_l^m$ straightforwardly using (87).

REFERENCES

[1] F. Rusek, D. Persson, B. K. Lau, E. G. Larsson, T. L. Marzetta, O. Edfors, and F. Tufvesson, "Scaling up MIMO: Oppertunities and challenges with very large arrays," *IEEE Signal Process. Mag.*, vol. 30, no. 1, pp. 40–60, Jan. 2013.

[2] T. L. Marzetta, "Noncooperative cellular wireless with unlimited numbers of base station antennas," *IEEE Trans. Wireless Commun.,* vol. 9, no. 11, pp. 3590–3601, Nov. 2010.

[3] H. Q. Ngo, E. G. Larsson, and T. L. Marzetta, "Energy and spectral efficiency of very large multiuser MIMO systems," *IEEE Trans. Commun.,* vol. 61, no. 4, pp. 1436–1449, Apr. 2013.

[4] E. G. Larsson, F. Tufvesson, O. Edfors, and T. L. Marzetta, "Massive MIMO for next generation wireless systems," *IEEE Commun. Mag.*, vol. 52, no. 2, pp. 186–195, Feb. 2014.

[5] J. Jose, A. Ashikhmin, T. L. Marzetta, and S. Vishwanath, "Pilot contamination and precoding in multi-cell TDD systems," *IEEE Trans. Wireless Commun.*, vol. 10, no. 8, pp. 2640–2651, Aug. 2011.

[6] A. Adhikary, J. Nam, J. Ahn, and G. Caire, "Joint spatial division and multiplexing – The large-scale array regime," *IEEE Trans. Inf. Theory*, vol. 59, no. 10, pp. 6441–6463, June 2013.

[7] H. Yin, D. Gesbert, M. Filippou, and Y. Liu, "A coordinate approach to channel estimation in large-scale multiple-antenna systems," *IEEE J. Sel. Areas Commun.*, vol. 31, no. 2, pp. 264–273, Feb. 2013.

[8] H. Q. Ngo and E. G. Larsson, "EVD-based channel estimation in multicell multiuser MIMO systems with very large antenna arrays," in *Proc. IEEE ICASSP*, Mar. 2012, pp. 3249–3252.

[9] F. Fernandes, A. Ashikhmin, and T. L. Marzetta, "Inter-cell inteference in noncoorperative TDD large scale antenna systems," *IEEE J. Sel. Areas Commun.*, vol. 31, no. 2, pp. 192–201, Feb. 2013.

[10] A. Ashikhmin and T. L. Marzetta, "Pilot contamination precoding in multi-cell large scale antenna systems," in *Proc. IEEE ISIT*, July 2012, pp. 1137–1141.

[11] E. Benner and A. Sesay, "Effects of antenna height, antenna gain, and pattern downtilting for cellular mobile radio," *IEEE Trans. Veh. Technol.*, vol. 45, no. 2, pp. 214–227, May 1996.

[12] I. Forkel, A. Kemper, R. Pabst, and R. Hermans, "The effect of electrical and mechanical antenna down-tilting in umts networks," in *Proc. IET Int. Conf. 3G Mobile Commun. Technol.*, May 2002, pp. 86–90.

[13] B. Partov, D. J. Leith, and R. Razavi, "Utility fair optimisation of antenna tilt angles in LTE networks," submitted to *IEEE/ACM Trans. Networking*, [Online] Available at: http://arxiv.org/abs/1310.1015.

[14] F. Athley and M. N. Johansson, "Impact of electrical and mechanical antenna tilt on LTE downlink system performance," in *Proc. IEEE VTC*, May 2010.

[15] N. Seifi, M. Coldrey, M. Matthaiou, and M. Viberg, "Impact of base station antenna tilt on the performance of network MIMO systems," in *Proc. IEEE VTC*, May 2012.

[16] O. N. C. Yilmaz, S. Hämäläinen, and J. Hämäläinen, "Analysis of antenna parameter optimization space for 3GPP LTE," in *Proc. IEEE VTC*, Sep. 2009.

[17] H. Eckhardt, S. Klein, and M. Gruber, "Vertical antenna tilt optimization for LTE base stations," in *Proc. IEEE VTC*, May 2011.

[18] R. Razavi, S. Klein, and H. Claussen, "A fuzzy reinforcement learning approach for self optimization of coverage in LTE networks," *J. Bell Lab. Tech.*, vol. 15, pp. 153–175, Dec. 2010.

[19] I. Rodriguez, H. C. Nguyen, T. B. Sørensen, and J. Elling, "A geometrical-based vertical gain correction for signal strength prediction of downtilted base station antennas in urban areas," in *Proc. IEEE VTC*, Sep. 2012.

[20] N. Seifi, M. Coldrey, and M. Viberg, "Throughput optimization for MISO interference channels via coordinate user-specific tilting," *IEEE Commun. Lett.*, vol. 16, no. 8, pp. 1248–1252, Aug. 2012.

[21] 3GPP TR 36.814 V9.0, "Further advancements for E-UTRA physical layer aspects," Tech. Rep., March 2010.

This article has been accepted for publication in a future issue of this journal, but has not been fully edited. Content may change prior to final publication. Citation information: DOI 10.1109/TVT.2014.2385878, IEEE Transactions on Vehicular Technology

[22] Y.-H. Nam, B. L. Ng, K. Sayana, Y. Li, J. Zhang, Y. Kim and J. Lee, "Full dimension MIMO (FD-MIMO) for next generation cellular technology," *IEEE Commun. Mag.,* vol. 51, no. 6, pp. 172–179, June 2013.

[23] T. Q. S. Quek, G. de la Roche, I. Guvenc, and M. Kountouris, "Small cell networks: Deployment, PHY techniques, and resource allocation," Cambridge University Press, 2013.

[24] R. Pabst *et. al.*, "Relay-based deployment concepts for wireless and mobile broadband radio," *IEEE Commun. Mag.*, vol. 42, no. 9, pp. 80–89, Sep. 2004.

[25] Y. Zhuang, Y. Luo, L. Cai, and J. Pan, "A geometric probability model for capacity analysis and interference estimation in wireless mobile cellular systems," in *Proc. IEEE GLOBECOM*, Dec. 2011.

[26] A. Goldsmith, *Wireless Communications*, Cambridge University Press, New York, 2005.

[27] A. Lozano, R. W. Heath Jr., and J. G. Andrews, "Fundamental limits of cooperation," *IEEE Trans. Inf. Theory*, vol. 59, no. 9, pp. 5213–5226, Sep. 2013.

Shi Jin (S'06-M'07) received the B.S. degree in communications engineering from Guilin University of Electronic Technology, Guilin, China, in 1996, the M.S. degree from Nanjing University of Posts and Telecommunications, Nanjing, China, in 2003, and the Ph.D. degree in communications and information systems from the Southeast University, Nanjing, in 2007. From June 2007 to October 2009, he was a Research Fellow with the Adastral Park Research Campus, University College London, London, U.K. He is currently with the faculty of the National Mobile Communications Research Laboratory, Southeast University. His research interests include space time wireless communications, random matrix theory, and information theory. He serves as an Associate Editor for the IEEE TRANSACTIONS ON WIRELESS COMMUNICATIONS, IEEE COMMUNICATIONS LETTERS, and IET COMMUNICATIONS. Dr. Jin and his co-authors have been awarded the 2011 IEEE Communications Society Stephen O. Rice Prize Paper Award in the field of communication theory and a 2010 Young Author Best Paper Award by the IEEE Signal Processing Society.

Jue Wang (S'10 - M'14) received the B.S. degree in communications engineering from Nanjing University, Nanjing, China, in 2006, the M.S. degree and Ph. D. degree from the National Communications Research Laboratory, Southeast University, Nanjing, China, respectively in 2009 and 2014.

In 2014, he joined the School of Electronic and Information Engineering, Nantong University. Meanwhile, he is with Singapore University of Technology and Design (SUTD) as a post-doctoral research fellow. His research interests include MIMO wireless communications, multiuser transmission, MIMO channel modeling, massive MIMO systems and physical layer security.

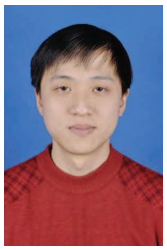

Qiang Sun (S'10) received the Ph.D. degree in Communication and Information System from Southeast University, Nanjing, China, in 2014. He joined the School of Electronic and Information Engineering, Nantong University, Nantong, China, in April 2006. Now he is a lecturer of information systems and communications. His current research interests include massive MIMO and small cell networks.

Michail Matthaiou (S'05–M'08–SM'13) was born in Thessaloniki, Greece in 1981. He obtained the Diploma degree (5 years) in Electrical and Computer Engineering from the Aristotle University of Thessaloniki, Greece in 2004. He then received the M.Sc. (with distinction) in Communication Systems and Signal Processing from the University of Bristol, U.K. and Ph.D. degrees from the University of Edinburgh, U.K. in 2005 and 2008, respectively. From September 2008 through May 2010, he was with the Institute for Circuit Theory and Signal Processing, Munich University of Technology (TUM), Germany working as a Postdoctoral Research Associate. He is currently a Senior Lecturer at Queen's University Belfast, U.K. and also holds an adjunct Assistant Professor position at Chalmers University of Technology, Sweden. His research interests span signal processing for wireless communications, massive MIMO, hardware-constrained communications, and performance analysis of fading channels.

Dr. Matthaiou is the recipient of the 2011 IEEE ComSoc Best Young Researcher Award for the Europe, Middle East and Africa Region and a co-recipient of the 2006 IEEE Communications Chapter Project Prize for the best M.Sc. dissertation in the area of communications. He was co-recipient of the Best Paper Award at the 2014 IEEE International Conference on Communications (ICC) and was an Exemplary Reviewer for IEEE COMMUNICATIONS LETTERS for 2010. He has been a member of Technical Program Committees for several IEEE conferences such as ICC, GLOBECOM, VTC etc. He currently serves as an Associate Editor for the IEEE TRANSACTIONS ON COMMUNICATIONS, IEEE COMMUNICATIONS LETTERS and was the Lead Guest Editor of the special issue on "Large-scale multiple antenna wireless systems" of the IEEE JOURNAL ON SELECTED AREAS IN COMMUNICATIONS. He is an associate member of the IEEE Signal Processing Society SPCOM and SAM technical committees.

Xiqi Gao (SM'07–F'14) received the Ph.D. degree in electrical engineering from Southeast University, Nanjing, China, in 1997. He joined the Department of Radio Engineering, Southeast University, in April 1992. Since May 2001, he has been a professor of information systems and communications. From September 1999 to August 2000, he was a visiting scholar at Massachusetts Institute of Technology, Cambridge, and Boston University, Boston, MA. From August 2007 to July 2008, he visited the Darmstadt University of Technology, Darmstadt, Germany, as a Humboldt scholar. His current research interests include broadband multicarrier communications, MIMO wireless communications, channel estimation and turbo equalization, and multirate signal processing for wireless communications. He serves as an Associate Editor for the IEEE TRANSACTIONS ON SIGNAL PROCESSING and the IEEE TRANSACTIONS ON WIRELESS COMMUNICATIONS. Dr. Gao received the Science and Technology Awards of the State Education Ministry of China in 1998, 2006 and 2009, the National Technological Invention Award of China in 2011, and the 2011 IEEE Communications Society Stephen O. Rice Prize Paper Award in the field of communications theory.